Inorganica Chimica Acta 447 (2016) 22–31

Contents lists available at ScienceDirect

Inorganica Chimica Acta

journal homepage: www.elsevier.com/locate/ica

Secondary interactions in decachloro-*closo*-decaborates $R_2[B_{10}Cl_{10}]$ ($R = Et_3NH^+$, Ph_4P^+, and $[Ag(NH_3)_2]^+$): ^{35}Cl NQR, PW-DFT, and X-ray studies

E.A. Kravchenko [a], A.A. Gippius [b,c], A.A. Korlyukov [d,e], A.V. Vologzhanina [d,*], V.V. Avdeeva [a,*], E.A. Malinina [a], E.O. Ulitin [b], N.T. Kuznetsov [a]

[a] Kurnakov Institute of General and Inorganic Chemistry, Russian Academy of Sciences, Leninskii pr. 31, 119991 Moscow, Russia
[b] Physics Department, Moscow State University, Leninskie Gory 1/2, 119991 Moscow, Russia
[c] Shubnikov Institute of Crystallography, Russian Academy of Sciences, Leninskii pr. 58, 119333 Moscow, Russia
[d] Nesmeyanov Institute of Organoelement Compounds, Russian Academy of Sciences, ul. Vavilova 28, 119991 Moscow, Russia
[e] Pirogov Russian National Research Medical University, ul. Ostrovityanova 1, 117997 Moscow, Russia

ARTICLE INFO

Article history:
Received 26 November 2015
Received in revised form 14 March 2016
Accepted 18 March 2016
Available online 25 March 2016

Keywords:
Decachloro-*closo*-decaborate anion
Perhalogenated boron cluster
^{35}Cl NQR spectroscopy
Specific interactions
X-ray diffraction

ABSTRACT

Three new salts $R_2[B_{10}Cl_{10}]$ ($R = Et_3NH^+$, Ph_4P^+, $[Ag(NH_3)_2]^+$, **1**–**3**) containing bulky decachloro-*closo*-decaborate dianion have been synthesized and characterized using the IR, ^{11}B NMR, and ^{35}Cl NQR spectroscopy. Neither IR nor ^{11}B NMR spectra have shown distinctions between compounds **1**–**3**, whereas ^{35}Cl NQR spectra of all the compounds have been split evidencing for crystallographic non-equivalence of chlorine atoms caused by secondary interactions. Crystal structures of **2** and **3** have been studied using X-ray diffraction and periodic DFT calculations, whereas unit cell parameters and space group of **1** have been estimated using powder X-ray diffraction. The ^{35}Cl NQR data supported by analysis of calculated electron density functions within the framework of Bader's Quantum Theory of Atoms in Molecules (QTAIM) showed that both cation and solvent molecules take part in N–H...Cl and C–H...Cl bonding as strong as 2.5 and 2.1 kcal/mol, respectively. The QTAIM study has revealed in **2** a number of p...π interactions between lone pairs of chlorine atoms and delocalized electron density of phenyl rings or C≡N groups of acetonitrile molecules, and the strongest of them (0.9 kcal/mol) has been reflected in the ^{35}Cl NQR spectrum. The results have shown that the halogen-substituted boron clusters can act as tags sensitive to H...Hal and p...π bonding, which can be identified by the NQR spectra even in the absence of structural data.

1. Introduction

Higher polyhedral boron cluster anions and carboranes [1] in numerous salts and complexes tend to form various multicentered specific interactions B–H...M or B–H...H(X) (X = C, N, O) with metals M, organic cations or solvent molecules [2]. Halogenated derivatives of boranes and carboranes are capable of producing, due to architectural variety of geometric shapes, macromolecules with unusual physicochemical properties. They are used as non-aqueous electrolytes for batteries since 1980s [3], as ionic liquids [4], weakly coordinating anions [5], the Brønsted superacids [6], and components in fuel cells [7]. Although Cl...H contacts were found by X-ray diffraction only in the carborane acid $H[CHB_{11}Cl_{11}]$ [7], specific non-valent (secondary) interactions are thought to be an important structure-forming factor for all the compounds. In contrast to B–H...X bonds, which can be revealed by the IR spectroscopy due to splitting of the ν(BH) band, the B–Cl...X bonds cannot be identified by this method because chlorine atoms are heavier, the bonding is weaker, and no changes in ν(BCl) band are observed in the IR-spectra.

Alcock [8] describes secondary bonds as the bonds, which are much longer than covalent and much shorter than the sum of van der Waals radii of corresponding atoms. No system exists however which unambiguously determines the van der Waals radii. Therefore, the choice of the experimental technique that allows one to select from the whole totality of interatomic contacts those associated with secondary interactions is an actual problem. Such technique is expected to detect subtle changes in electron density redistribution, which occur upon weak bonding between

* Corresponding authors.
E-mail addresses: vologzhanina@mail.ru (A.V. Vologzhanina), avdeeva.varvara@mail.ru (V.V. Avdeeva).

http://dx.doi.org/10.1016/j.ica.2016.03.025
0020-1693/

atoms-partners. Most spectroscopic techniques cannot reliably detect these changes however.

It is known that the configuration of the boron cage in the stable $[B_{10}Cl_{10}]^{2-}$ cluster, whose salts and complexes may be promising compounds for the ^{35}Cl nuclear quadrupole resonance (NQR) spectroscopy, is a bicapped square Archimedean antiprism with 8 equatorial and 2 apical chlorine atoms (Fig. 1). To our knowledge, neither the charge density in the anion nor ^{35}Cl NQR data for compounds containing the $[B_{10}Cl_{10}]^{2-}$ dianion are available in the literature. A hypothetical ^{35}Cl NQR spectrum of such an isolated anion should be a doublet with 4:1 intensity ratio.

Due to the high sensitivity of NQR spectroscopic parameters to the peculiarities of electronic distribution, geometry and stereochemistry of compounds, the method is recognized as an effective instrument for studying various solids including glasses, inclusion compounds, porous materials, films, etc [9]. It is obvious that involvement of the chlorine atoms in secondary interactions will cause their non-equivalence due to the electron density redistribution. As a result, the splitting of the resonances is expected. For chemically equivalent atoms in the crystallographically non-equivalent positions, the spectroscopic splitting is caused by the crystal field effects, which include contributions to the electric field gradient (EFG) of secondary interactions. This splitting rarely exceeds 5% [10]. Other characteristics of NQR spectra (frequency shift, multiplicity, line width, temperature dependence of resonance frequencies) also yield an information about basic structural features of compounds [9].

Information on chemistry of the decachloro-*closo*-decaborate anion, which can be found in the literature, is fragmented. Salts $Cat_2[B_{10}Cl_{10}]$ (Cat = Li,[3] K,[11] imidazole cations[4]) and acid $(H_3O)_2[B_{10}Cl_{10}]$ [7] were described as well as the ability of the $[B_{10}Cl_{10}]^{2-}$ anion to form radical ion [12] $[B_{10}Cl_{10}]^{\cdot-}$ in the presence of oxidizing agents. According to the results of IR spectroscopy [13] and X-ray diffraction studies [14] of cobalt(II) complexes with phenanthroline $[Co(phen)_3][B_{10}Cl_{10}]$ and $[Co_2(phen)_4][B_{10}Cl_{10}]$, the perchlorinated *closo*-decaborate anion is the outer sphere anion. Neither complexes with other metals nor functionalized halogenated derivatives are known.

It should be noted that the experimental methods traditionally used (IR and UV spectroscopy, X-ray diffraction) could not conclusively reveal the presence of specific interactions in compounds with $[B_{10}Cl_{10}]^{2-}$. However, these specific interactions were identified by ^{35}Cl NQR spectroscopy: the H...Cl hydrogen bonds were found in CCl_4 clathrates [15] and pharmaceuticals [16], weak Ag...Cl bonds—in silver halomethanesulfonates [17], and p...π bonding—in Menshutkin molecular compounds {(arene)·nSbX$_3$} (X = Cl, Br) [18]. As to the theoretical approaches for identification of secondary interactions, the most prominent one for identification of secondary interactions is the quantum theory of atoms-in-molecules based on topological analysis of the experimental or calculated electron density $\rho(\mathbf{r})$ (QTAIM) [19]. By this approach, the interactions can be identified based on the analysis of the electron density gradient as bond critical points (BCP), followed by evaluation of the interaction strength (E_{int}) from the electron density values and the Laplacian in BCP. According to the QTAIM, the C–H...Cl and Cl...Cl bonds were found to be the closed-shell interactions of mainly electrostatic nature with E_{int} varying from −1.5 to −15.5 kcal/mol [20]. Recently, combination of the QTAIM and ^{14}N NQR was successfully applied to investigate polymorphism and hydrogen bonding in solid 1,2,3-thiadiazole derivatives [21].

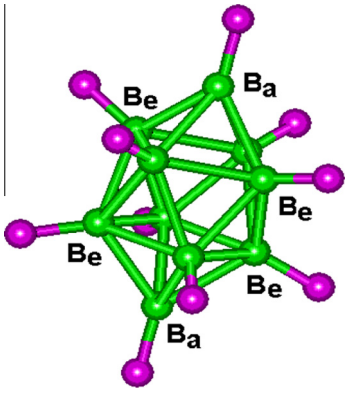

Fig. 1. Structure of the decachloro-*closo*-decaborate anion $[B_{10}Cl_{10}]^{2-}$; B_a and B_e are apical and equatorial atoms, respectively.

To clarify the nature of specific bonding in decahydro-*closo*-decaborates, compounds $R_2[B_{10}Cl_{10}]$ (where R = Et_3NH^+, Ph_4P^+, $[Ag(NH_3)_2]^+$, (**1**–**3**)) were prepared and studied using ^{35}Cl NQR spectroscopy and X-ray diffraction. PW-DFT calculations and QTAIM analysis of **2** and **3** were carried out to estimate energies of secondary interactions. The results yielded an information on the effect of cations (organic or complex), temperature, and preparation procedures on the ability of the $[B_{10}Cl_{10}]^{2-}$ anion to form secondary bonds.

2. Results and discussion

*2.1. Synthesis of compounds $R_2[B_{10}Cl_{10}]$, where R = Et_3NH^+ (**1**), Ph_4P^+ (**2**), and $[Ag(NH_3)_2]^+$ (**3**)*

The chemistry of decachloro-*closo*-decaborate anion was insufficiently studied and scarcely described in the literature. In contrast to a variety of chemical properties of the parental decahydro-*closo*-decaborate anion $[B_{10}H_{10}]^{2-}$ [1], which can act as inner-sphere ligand, participate in numerous substituted reactions, and posses reduction activity, the perhalogenated analog was only found to form salts $Cat_2[B_{10}Cl_{10}]$ [3,4,7,11], act as counter ion in cobalt(II) complexes with phenanthroline [13,14], and form $[B_{10}Cl_{10}]^{\cdot-}$ radical ion [12]. It is known that silver tends to form bonds with chlorine atoms; particularly, the crystal structure of solvent-free dodecachloro-*closo*-dodecaboratosilver(I) $[Ag_2[B_{12}Cl_{12}]]$ was reported [22]. The latter was prepared by interaction of $AgNO_3$ with $Cs_2[B_{12}Cl_{12}]$ in aqueous solution. Each silver atom is coordinated by six chlorine atoms providing a distorted octahedral coordination sphere of the Ag^+ cations, the Ag–Cl distances falling in the range of 2.83–2.85 Å. The presence of specific Ag...Cl interactions was not confirmed by other physicochemical methods.

In order to find specific interactions in decachloro-*closo*-decaboratosilver(I), we prepared silver(I) complex $[Ag(NH_3)_2]_2[B_{10}Cl_{10}]$ (**3**) by reaction between $[HNEt_3]_2[B_{10}Cl_{10}]$ (**1**), aqueous $AgNO_3$, and a solution of NH_3 H_2O according to Scheme 1.

The desired product **3** precipitated in the crystalline form from the reaction mixture after 24 h. In the IR spectra of the complex, there are two intense absorption bands corresponding to ν(BCl) stretching vibrations with maxima at 1163 and 1003 cm^{-1}. In the IR spectra of the previously studied complexes $[Co(phen)_3][B_{10}Cl_{10}]$ and binuclear $[Co_2(\mu\text{-}Cl)_2(phen)_4][B_{10}Cl_{10}]$, the maxima of the ν(BCl) bands were found at 1145, 1003 and 1147, 1003 cm^{-1}, respectively. The shape and intensities of the bands were identical, and we could not say from the IR spectroscopy data if any specific interactions are present in the cobalt complexes or in compound **3**. At the same time, the ν(BH) band in the IR spectra of decahydro-*closo*-decaborates with specific B–H...H–X interactions (X = C, O, N,) (dihydrogen bonds) is shifted to 100 cm^{-1} hence making this method an express-instrument for identification of compounds with the B–H...H–X interactions. It is clear that more information is necessary for clarifying the nature of specific interactions in compounds with perhalogenated *closo*-decaborate anion.

$$[HNEt_3]_2[B_{10}Cl_{10}]\ (\mathbf{1}) + 2\ AgNO_3 + 4\ NH_3{\cdot}H_2O \xrightarrow{H_2O} [Ag(NH_3)_2]_2[B_{10}Cl_{10}]\downarrow\ (\mathbf{3}) + 2\ [HNEt_3]NO_3$$

Scheme 1. Preparation of silver(I) complex **3**.

$$K_2[B_{10}Cl_{10}] + 2[HNEt_3]Cl \xrightarrow{H_2O} [HNEt_3]_2[B_{10}Cl_{10}]\downarrow\ (\mathbf{1}) + 2KCl$$

Scheme 2. Preparation of salt **1**.

For comparison, we studied the IR-spectra of ammonium $[Et_3NH]_2[B_{10}Cl_{10}]$ (**1**) and phosphonium $[Ph_4P]_2[B_{10}Cl_{10}]$ (**2**) salts. The compound **1** was synthesized by interaction of potassium decachloro-*closo*-decaborate by the interaction with aqueous $[HNEt_3]Cl$ (Scheme 2).

Compound **2** was prepared by exchange reaction between compound **1** and tetraphenylphosphonium chloride (Scheme 3) in aqueous solution. Both compounds precipitated from the reaction solutions as powders.

Crystals **2**·3CH_3CN were obtained by recrystallization of precipitate **2** from acetonitrile. In the IR spectra of compounds **2** and **3**, ν(BCl) bands were observed with maxima at 1158, 999 and 1156, 1003 cm^{-1}, respectively. As IR spectroscopy gives no information about specific interactions in the compounds discussed, compounds **1**–**3** were studied using X-ray diffraction and ^{35}Cl NQR spectroscopy.

2.2. Structure, QTAIM analysis, and ^{35}Cl NQR spectrum of $[Ag(NH_3)_2]_2[B_{10}Cl_{10}]$ (3)

According to our X-ray diffraction data, $[Ag(NH_3)_2]_2[B_{10}Cl_{10}]$ (**3**) crystallizes in the orthorhombic system (sp. gr. *Pbcn*) with only a half of anion and one cation in the asymmetric unit (Fig. 2). The characteristics of intramolecular bonds are listed in Table 1.

PW-DFT geometry reproduced fairly well the experimental molecular geometry with the exception of normalized N–H distances and Ag–N bonds. The $[Ag(NH_3)_2]^+$ cation is equal-armed and almost linear (178.9°) in the theoretical model, while the experimental Ag–N bonds differ from each other. At the same time, the N1...N2 distance remains unchanged (4.267 and 4.266 Å for experimental and calculated geometries). The QTAIM analysis of the theoretical electron density $\rho(\mathbf{r})$ revealed all the expected BCPs for Ag–N, H–N, Cl–B, and B_a–B_e interactions, although some of B_e–B_e bonds are absent. This fact is referred to the electron density delocalization over the surface of polyhedral borane clusters [23] and was previously observed for $[B_{10}H_{10}]^{2-}$ in $(Hbipy)_2[B_{10}H_{10}]$ [24] and $[Cu_2(bipy)_2B_{10}H_{10}]$ [25]. Characteristics of electron density in BCPs are very close to those for the borane family (Table 1) [26] and match the correlation $\rho(\mathbf{r})$ *vs.* B–B bond distance, which was found for other boron clusters [24]. At BCPs, differences of $\rho(\mathbf{r})$ values assigned to the B_a–B_e and B_e–B_e bond distances in the perchlorinated $[B_{10}Cl_{10}]^{2-}$ anion from those in the $[B_{10}H_{10}]^{2-}$ dianion are accounted for the effect of chlorine atoms and pronounced difference in bond distances. Nevertheless, negative values of $\nabla^2\rho(\mathbf{r})$ and $h_e(\mathbf{r})$ undoubtedly indicate that all B–B and N–H interactions are shared interactions, e.g. covalent non-polar or slightly polar interactions, whereas all Ag–N and Cl–B interactions ($\nabla^2\rho(\mathbf{r}) > 0$ and $h_e(\mathbf{r}) < 0$) are highly polar covalent bonds with significant ionic contribution.

At last, the QTAIM revealed the presence of a number of the closed-shell Ag...Cl, N–H...Cl and Cl...Cl interactions (those with positive $\nabla^2\rho(\mathbf{r})$ and $h_e(\mathbf{r})$ are here specific bonds) (Table 2). Particularly, the coordination environment of silver cation in crystal can be described as 2 + 5 pentagonal bipyramid with five chlorine atoms in the equatorial plane (Fig. 2b).

The Ag–N binding energies, estimated using the EML correlation $E_{int} \approx -1/2\ V^e(\mathbf{r})$ [27], give the E_{int} values equal to 45.5 kcal/mol. Although the correlation was derived for hydrogen bonds, its correctness was later demonstrated for intermediate interactions containing transition metals [28]. In **3**, the estimated value of E_{int} correlates with binding energies of 40.6(18) and 47.5(16) kcal/mol reported by El Aribi et al. [29] and Deng & Kebarle [30]. The energies of Ag...Cl interactions estimated using the EML correlation do not exceed 2.4 kcal/mol. The E_{int} values for some of the N–H...Cl interactions achieve 2.5 kcal/mol, while those for halogen interactions (Cl...Cl) vary from 0.3 to 0.9 kcal/mol. As one expects, the shorter the intermolecular distance, the higher the E_{int} value, so that the interactions with significantly non-zero E_{int} (>1.5 kcal/mol) are also characterized by distances much shorter than the sum of their van der Waals radii, e.g. they undoubtedly belong to secondary interactions. The chlorine atoms involved in the relatively strong N–H...Cl interactions are the apical Cl1 atom and one equatorial Cl2 atom (Fig. 3, Table 2). Due to H-bonding, each anion coordinates six different cations, and each cation is connected with three anions (Fig. 3). The resulting H-bonded net obtained within the ToposPro package [31] as simplification of cations and anions to their centers of gravity keeping connectivity of the net belongs to the α-PbO_2 topological type.

Integrating the electron density over the surface of zero-flux gives the charges of +0.65 and −1.30 e on $[Ag(NH_3)_2]^+$ and $[B_{10}Cl_{10}]^{2-}$, respectively, while both NH_3 molecules are almost neutral (+0.05 and +0.09 e). The majority of the interactions seem to occur between negatively charged chlorine atoms and positively charged hydrogen and silver atoms (Table S1).

As was said above, a weakly split doublet with an intensity ratio of 4:1 is expected in the ^{35}Cl NQR spectra of the $[B_{10}Cl_{10}]^{2-}$ dianion (from 8 equatorial and 2 apical chlorine atoms) in the absence of secondary bonds. Three lines were however detected in the ^{35}Cl NQR spectrum of **3** at 19 K (Fig. 4). It is important to note that the ^{35}Cl NQR spectra of **1**–**3** could be observed only after cooling the samples to 19 K. We could also observe the spectrum of **1** at 77 K, but a thorough search of the ^{35}Cl resonances at room temperature gave no results for all the samples. The origin of these two low-frequency lines can be accounted for the involvement of the Cl1 and Cl2 atoms to the N–H...Cl bonding (Table 2).

The Cl3 atom has two Ag atoms at distances which are shorter than the sum of van der Waals radia (3.75 Å) [29] (Fig. 3). The evaluation of the relative additions to the q_{zz} values at the Cl3, Cl2 and Cl1 atoms from their neighboring atoms at the shortened distances (these are proportional to

$$\sum_i e\rho_i(3\cos 2\theta_i - 1)/R_i^3$$

where θ_i is the angle H(Ag)...Cl–B, R_i is the H(Ag)...Cl_i distances and ρ_i is the effective charge on the Ag(H) atoms) shows, that the addition of Ag...Cl3 to the EFG at Cl3 is much smaller than similar additions to the EFG at the Cl2 and Cl1 atoms from hydrogen atoms (roughly as 1:6:8, respectively). Hence, the appropriate frequency shift due to the secondary interactions Cl3...Ag seems to fall within the line width of the resonance ν = 22.2 MHz (Fig. 4).

$$[HNEt_3]_2[B_{10}Cl_{10}]\ (\mathbf{1}) + 2[Ph_4P]Cl \xrightarrow{H_2O} [Ph_4P]_2[B_{10}Cl_{10}]\downarrow\ (\mathbf{2}) + 2[HNEt_3]Cl$$

Scheme 3. Preparation of salt **2**.

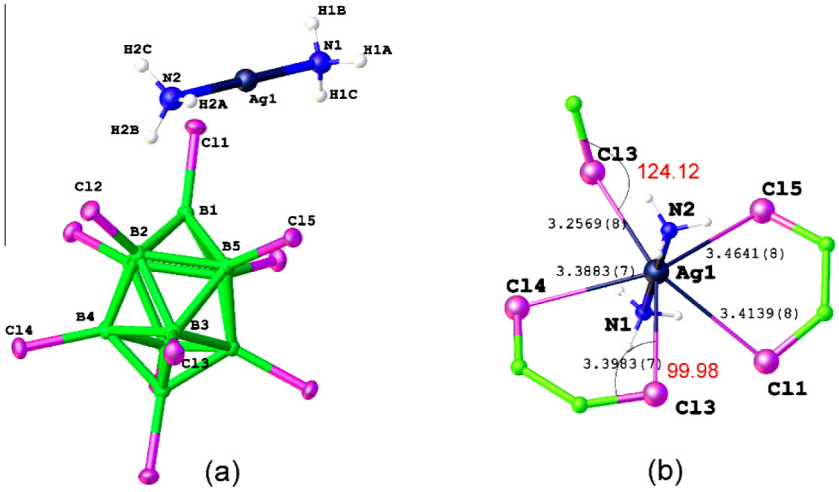

Fig. 2. (a) Molecular view of asymmetric unit of **3** in representation of atoms with thermal ellipsoids; (b) coordination environment of silver atoms (selected bond distances (Å) and angles (°) are depicted with black and red, respectively). (For interpretation of the references to color in this figure legend, the reader is referred to the web version of this article.)

Table 1
QTAIM properties of intramolecular bonds in **3**.[a]

Bond	r_{exp}(A–Z)	r_{theor}(A–Z)	$\rho(\mathbf{r})$	$\nabla^2\rho(\mathbf{r})$	$V^e(\mathbf{r})$	$h_e(\mathbf{r})$	E_{int}	av
av. Ag–N	2.128(3)–2.140(3)	2.133	0.64	8.37	−0.145	−0.028	45.5	2
av. B_a–B_e	1.687(4)	1.690	0.93	−4.71	−0.198	−0.123		4
av. B_e–B_e	1.840(4)	1.833	0.76	−2.65	−0.143	−0.085		5
Cl–B_a	1.790(3)	1.789	0.90	2.65	−0.211	−0.092		1
av. Cl–B_e	1.800(3)	1.803	0.90	0.93	−0.205	−0.097		4
av. N–H	0.910	1.023	2.30	−48.73	−0.797	−0.653		6

[a] r_{exp}(A–Z) and r_{theor}(A–Z) are experimental and theoretical interatomic distances (Å); $\rho(\mathbf{r})$ – the ED at the BCP (e Å^{-3}); $\nabla^2\rho(\mathbf{r})$ – the corresponding Laplacian (in e Å^{-5}); $V^e(\mathbf{r})$ – the potential energy density (a.u.); $h_e(\mathbf{r})$ – the local energy density (a.u.); E_{int} – energy for a intermolecular bond estimated using the ESM correlation (kcal/mol); av – the number of averaged data.

Meanwhile, X-ray studies of **3** point to the presence of short N–H…Cl (<2.95 Å) and Ag…Cl (<3.5 Å) contacts for all the chlorine atoms without exception (Table 2). It is not excluded that the contacts that are not reflected in the NQR spectra lie within the inaccuracy of determining the van der Waals radii in the Bondi system used for classifying the interatomic distances [32]. As to the ratio of the line intensities, the reason for deviation of the recorded signals (Fig. 4) from the ratio of intensities 1:1:3, which follows from the structural data, may be, in addition to differences in relaxation times, the differences in probabilities of the corresponding transitions, which in turn depend on the values of the EFG asymmetry parameters η [33]. Unfortunately, technical limitations of the equipment, used in this experiment, did not allow us to measure the values of η (see Section 5).

2.3. Structure, QTAIM analysis, and ^{35}Cl NQR spectrum of $(Ph_4P)_2[B_{10}Cl_{10}]$ (**2**)

The results of the X-ray diffraction showed that compound **2** crystallizes as associate with solvent molecules as **2**·3CH_3CN. This composition resulted in the formation of not only C–H…Cl, but also C–H…π and p…π bonding, where p is the lone pair of a chlorine atom. Previously, the existence of p…π bonding in a series of Menshutkin's {(arene)·n$SbCl_3$} molecular compounds was revealed using ^{35}Cl NQR [18]. The 5p_π(I)…π bonding in the complexes of dialkyl/diphenyldiiodostannates(IV) was also found using ^{127}I NQR [34].

Asymmetric unit of **2**·3CH_3CN is depicted in Fig. 5, characteristics of the intramolecular bonds and selected intermolecular interactions (those with interatomic distances shorter than the sum of van der Waals radii in the Bondi system) are listed in Tables 3 and 4, respectively. Asymmetric unit contains two cations, one anion and three solvate acetonitrile molecules. All BCPs were found for P–C, C–C, N–C and C–H bonds; the molecular graphs of the $[B_{10}Cl_{10}]^{2-}$ anion in **1** and **2** are similar (with eight missing B_e–B_e BCPs). As one can see from Table 3, the intramolecular bonds in **2**, except highly polar Cl–B interactions, are the shared interactions. Characteristics of chemical bonds for the cage dianion in **1** and **2** are very close to each other, but their overall QTAIM charges are slightly different (−1.30 and −1.45 e). The PPh_4^+ and MeCN bear on average +0.75 and +0.13 e, respectively (Table S2).

The QTAIM analysis of specific bonds in **2** revealed the C–H…Cl, Cl…Cl and p…π interactions (either with phenyl rings or the C≡N fragment). Besides, a number of C–H…π, π…π and C–H…H–C interactions were detected. All specific bonds are associated with the closed-shell interactions, the characteristics of the strongest bonds, which are shorter than the sum of van der Waals radii of corresponding elements, are listed in Table 4 and depicted in Fig. 6. The complete list of specific bonds for the chlorine atoms is given as Supplementary Information (Table S3). We found that only one apical and four equatorial chlorine atoms take part in interactions with E_{int} > 1.5 kcal/mol (C–H…Cl bond) and 1.0 kcal/mol (p…π bonding) (or with intermolecular distances 0.1 Å shorter than the sum of van der Waals radii of elements in the Bondi system). The C–H…Cl hydrogen bonds in **2** are weaker than N–H…Cl interactions in **3**, although they are still stronger than other specific bonds in **2**. Worth noting that the bulky $[B_{10}Cl_{10}]^{2-}$ anions form in crystals of both **2** and **3** the distorted body-centered

Table 2
QTAIM properties of intermolecular bonds in **3**.[a]

Atom A	Atom Z[b]	r_{exp}(A–Z)	r_{theor}(A–Z)	$\rho(\mathbf{r})$	$\nabla^2\rho(\mathbf{r})$	$V^e(\mathbf{r})\times10^3$	$h_e(\mathbf{r})\times10^3$	E_{int}	Δ
Cl1	Ag1^{i}	3.414	3.447	0.06	0.598	−4.6	0.9	1.44	−0.06
	Cl3^{ii}	3.718	3.720	0.03	0.383	−2.0	0.9	0.62	0.22
	H1A^{iii}	**2.786**	**2.609**	**0.08**	**0.789**	**−6.0**	**1.2**	**1.89**	**−0.16**
	H1C^{i}	**2.819**	**2.728**	**0.06**	**0.765**	**−5.2**	**1.4**	**1.62**	**−0.13**
	H2C^{iv}	**2.717**	**2.499**	**0.09**	**0.980**	**−7.8**	**1.1**	**2.46**	**−0.23**
Cl2	Cl4^{v}	3.890	3.859	0.02	0.287	−1.5	0.8	0.47	0.39
	Cl2^{v}	3.635	3.639	0.04	0.454	−2.7	1.0	0.86	0.14
	H1A^{iii}	2.919	2.821	0.06	0.693	−4.5	1.4	1.42	−0.03
	H1B^{vi}	**2.611**	**2.483**	**0.09**	**0.956**	**−7.9**	**1.0**	**2.49**	**−0.34**
	H2B^{i}	**2.687**	**2.562**	**0.08**	**0.813**	**−6.2**	**1.2**	**1.96**	**−0.26**
Cl3	Ag1^{vii}	3.257	3.232	0.09	0.909	−7.7	0.9	2.42	−0.21
	Ag1^{viii}	3.398	3.430	0.07	0.622	−4.8	0.8	1.50	−0.07
	Cl1^{ix}	3.718	3.720	0.03	0.383	−2.0	0.9	0.63	0.22
Cl4	Ag1^{viii}	3.388	3.395	0.07	0.670	−5.2	0.8	1.63	−0.08
	Cl2^{v}	3.890	3.859	0.02	0.287	−1.5	0.8	0.47	0.39
	H1C^{x}	2.947	2.802	0.06	0.574	−3.9	1.1	1.23	−0.003
	H2C^{xi}	3.303	3.439	0.01	0.167	−0.7	0.5	0.24	0.35
Cl5	Ag1^{i}	3.464	3.461	0.06	0.574	−4.3	0.8	1.36	−0.01
	Cl5^{i}	3.623	3.579	0.02	0.215	−1.0	0.6	0.33	0.12
	H2A^{vii}	2.979	2.758	0.06	0.550	−3.8	0.9	1.20	0.03
	H2A^{xii}	2.832	2.729	0.06	0.670	−4.6	1.2	1.44	−0.12

[a] r_{exp}(A–Z) and r_{theor}(A–Z) are experimental and theoretical interatomic distances (Å); $\rho(\mathbf{r})$ – the ED at the BCP (e Å^{-3}); $\nabla^2\rho(\mathbf{r})$ – the corresponding Laplacian (in e Å^{-5}); $V^e(\mathbf{r})$ – the potential energy density (a.u.); $h_e(\mathbf{r})$ – the local energy density (a.u.); E_{int} – energy for a intermolecular bond estimated using the EML correlation (kcal/mol); Δ – the difference between experimental interatomic distance and van der Waals radii of corresponding elements. The Cl atoms involved, according to ^{35}Cl NQR, in secondary interactions are given in bold.

[b] Symmetry codes : (i) 1 − *x*, *y*, 3/2 − *z*; (ii) −1/2 + *x*, 3/2 − *y*, 2 − *z*; (iii) 1/2 + *x*, 1/2 + *y*, 5/2 − *z*; (iv) −1/2 + *x*, 3/2 − *y*, 1 − *z*; (v) 1 − *x*, 1 − *y*, 2 − *z* (vi) 3/2 − *x*, 3/2 − *y*,1 + *z* (vii) 1/2 + *x*, 5/2 − *y*, 1 − *z* (viii) 3/2 − *x*, 3/2 − *y*, 1/2 + *z*; (ix) 1/2 + *x*, 3/2 − *y*, 2 − *z*; (x) 5/2 − *x*,1/2 + *y*, *z*; (xi) *x*, 1 − *y*, 3/2 + *z*; (xii) 1 − *x*, 2 − *y*, 1 − *z*.

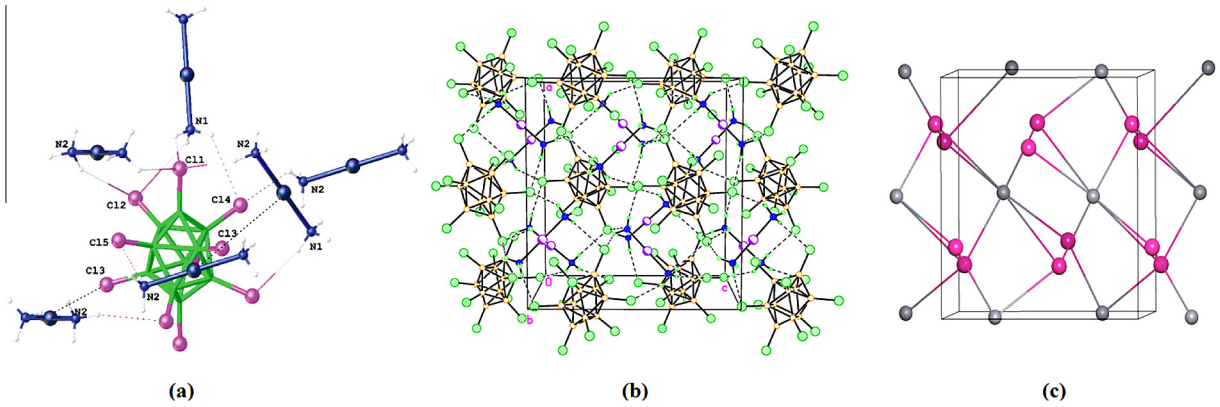

Fig. 3. (a) Intermolecular environment of cluster anion in **3**. Secondary interactions are depicted with dashed lines; (b) Fragment of crystal packing of **3** (view along crystallographic axis *b*). Hydrogen bonds are depicted with dashed lines; (c) The underlying net for H-bonded motif in **3** (view along crystallographic axis *b*). Gray spheres: centers of $B_{10}Cl_{10}^{2-}$; magenta: centers of $[Ag(NH_3)_2]^+$. (For interpretation of the references to color in this figure legend, the reader is referred to the web version of this article.)

cubic lattice with 14 neighboring anions around a given one. Steric hindrances from $[PPh_4]^+$ cation cause elongation of distances between centers of anions from 8.8–11.9 (for **3**) to 10.8–16.1 Å, although do not prevent the anions to form Cl...Cl interactions. The latter in **2** (3.517–3.618 Å) are even shorter than those in **3** (3.623–3.980 Å).

Although the energies of Cl...C and Cl...N interactions, which represent the p...π contacts, do not exceed 0.9 and 0.4 kcal/mol, the ^{35}Cl NQR reveals in **2**·3CH_3CN five chlorine atoms involved in strong secondary interactions (Fig. 7). This means that Cl...C interactions as short as 3.351 Å are reflected in the ^{35}Cl NQR spectrum. Certainly, the measurement of the EFG asymmetry parameter on the appropriate chlorine atom could provide a more definitive conclusion about the existence of p...π interactions. However, the ^{35}Cl NQR spectral pattern (Fig. 7) demonstrates the technical infeasibility of such an experiment. Apart from the instrumental reason described in Section 5, the high multiplicity of the signal with closely spaced components would not enable one to analyze an individual spin-echo envelope, which is necessary for the evaluation of the EFG asymmetry parameter. Meanwhile, the X-ray data point to the B–Cl...H shortened contacts for three more Cl atoms (Table 4).

*2.4. Spectroscopic evidences of secondary interactions in $(Et_3NH)_2[B_{10}Cl_{10}]$ (**1**)*

The IR spectrum of compound **1** contains absorption bands corresponding to *ν*(BCl) and *ν*(NH) stretching vibrations (see Section 5). As it was indicated, the shape and location of the *ν*(BCl) bands are equal to those observed for **2** and **3**, so that no differences between three spectra were found. In addition, the ^{11}B NMR spectrum of a solution of **1** in $[D_7]$DMF is similar to the ^{11}B NMR spectra of compounds **2** and **3**; specific interactions cannot be found by this method because of dissociation of salts in solution.

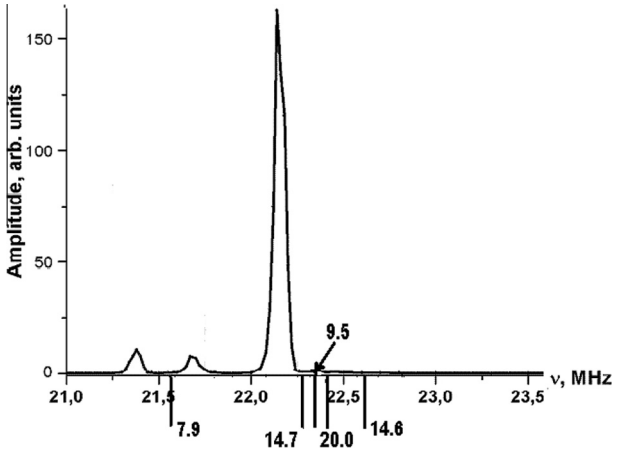

Fig. 4. The ^{35}Cl NQR spectrum of **3** at 19 K. The resonance frequencies estimated from PW-DFT data are shown as negative rods on the recordings of the experimental spectrum. For some rods, the EFG asymmetry parameters (η, %) are also given.

Therefore, both spectroscopic methods do not reveal specific interactions in compounds **1**–**3**.

Compound **1** has not been characterized by single crystal X-ray diffraction, but its composition makes highly probable the existence of secondary N–H...Cl and C–H...Cl interactions. Indeed, the widely split ^{35}Cl NQR spectrum was observed (Fig. 8, *a*) for the sample cooled to 19 K. Its line multiplicity exceeded 10 indicating the existence of several crystallographic types of cluster anions and at least 12 Cl atoms involved in secondary interactions in the crystal lattice. We could also observe the spectrum of **1** at 77 K, which unexpectedly showed no shift from the frequency range at 19 K (Fig. 8, *b*). The only difference between the two spectra was some broadening of the resonance lines observed for the heated sample. However, the effect of temperature on the ^{35}Cl NQR spectra and relationship between the spectrum and the peculiarities of the lattice dynamics seems to be rather complicated for this compound, taking into account the large number of secondary interactions suggested by the ^{35}Cl NQR spectral patterns. It requires special experiments, including relaxation studies.

To confirm the presence of non-equivalent $[B_{10}Cl_{10}]^{2-}$ anions in the crystal lattice and to estimate the composition of compound **1**, the powder X-ray diffraction study of the sample was carried out (Fig. 9). The powder X-ray diffraction pattern was successfully indexed to give the unit cell parameters: a = 26.3857 Å, b = 10.3570 Å, c = 30.3518 Å, β = 123.43°, V = 6406.5 Å^3 in the $P2_1/c$ space group (R_{Bragg} = 0.068, R_{wp} = 2.50). The data obtained indicate not only the purity of the sample, but also the presence of four crystallographically independent cations and two crystallographically independent anions. Indeed, Z = 4 for this space group and approximately 20 Å^3 per non–hydrogen atom and 2 Å^3 per each hydrogen atom give c.a. 6000 Å^3 for salt $(Et_3NH)_2[B_{10}Cl_{10}]$ at Z' = 2 and c.a. 400 Å^3 of extra volume which can be accounted for disorder of alkyl groups of bulky cations. Hence, not only C–H...Cl interactions but also N–H...Cl bonds can exist in this compound, which are responsible for the splitting of the ^{35}Cl NQR spectrum. Unfortunately, the complexity of the composition did not allow us to solve this structure.

3. Discussion

The titled compounds **1**–**3** are anion-cation salts with cations of essentially different sizes and properties. Therefore, the effect of external charges on the electron distribution within the complex anion is an important question. Such an effect was systematically analyzed using ^{35}Cl NQR spectroscopy for hexachlorometallates $R_2M^{IV}Cl_6$ (M^{IV} = Sn, Pb, Te, Pt, Re; R = K^+, Rb^+, Cs^+, NH_4^+, Me_4N^+) with

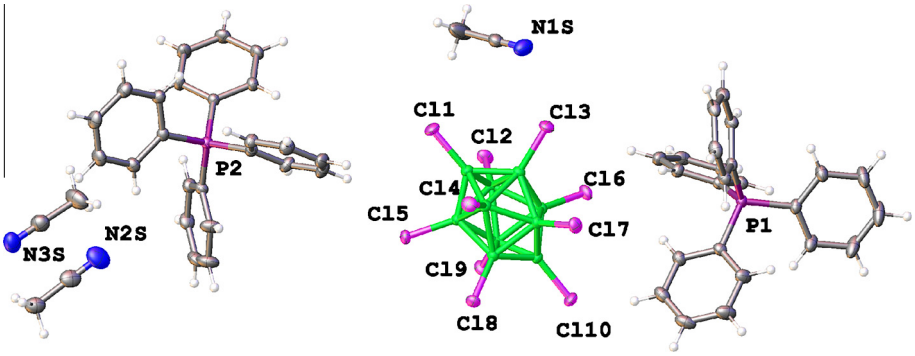

Fig. 5. Asymmetric unit of **2**·3CH_3CN in representation of atoms with thermal ellipsoids (drawn at p = 50%).

Table 3
QTAIM properties of selected intramolecular bonds in **2**·3CH_3CN.[a]

Bond	r_{exp}(A–Z)	r_{theor}(A–Z)	$\rho(\mathbf{r})$	$\nabla^2\rho(\mathbf{r})$	$V^e(\mathbf{r})$	$h_e(\mathbf{r})$	av
av. P–C	1.793(1)	1.800	1.19	−7.03	−0.298	−0.186	8
av. C_{Ph}–C_{Ph}	1.392(2)	1.398	2.10	−21.71	−0.749	−0.488	48
av. B_a–B_e	1.688(2)	1.691	0.93	−4.61	−0.197	−0.123	8
av. B_e–B_e	1.836(2)	1.832	0.76	−2.59	−0.142	−0.085	16
av. Cl–B_a	1.782(1)	1.786	0.91	2.49	−0.213	−0.093	2
av. Cl–B_e	1.800(1)	1.804	0.90	1.02	−0.205	−0.096	8
av. C–H	0.950	1.090	1.93	24.4	−0.632	−0.444	40

[a] r_{exp}(A–Z) and r_{theor}(A–Z) are experimental and theoretical interatomic distances (Å); $\rho(\mathbf{r})$ – the ED at the BCP (e Å^{-3}); $\nabla^2\rho(\mathbf{r})$ – the corresponding Laplacian (in e Å^{-5}); $V^e(\mathbf{r})$ – the potential energy density (a.u.); $h_e(\mathbf{r})$ – the local energy density (a.u.); av – the number of averaged data.

Table 4
QTAIM properties (a.u.) of selected intermolecular specific interactions in **2**·3CH_3CN.[a]

Atom A	Atom Z[b]	r_{exp}(A-Z)	r_{theor}(A–Z)	$\rho(\mathbf{r})$	$\nabla^2\rho(\mathbf{r})$	$V^e(\mathbf{r})\times10^3$	$h_e(\mathbf{r})\times10^3$	E_{int}	Δ_{BONDI}
Cl1	**H4SA^{i}**	2.864	2.697	**0.07**	**0.639**	**−4.8**	**0.9**	**1.52**	**−0.10**
	H2SA	2.737	2.644	**0.07**	**0.694**	**−5.3**	**1.0**	**1.67**	**−0.21**
Cl2	**H24^{ii}**	2.828	2.667	**0.07**	**0.067**	**−5.1**	**1.0**	**1.60**	**−0.12**
Cl3	H3	2.887	2.730	0.06	0.058	−4.2	0.9	1.35	−0.06
Cl4	H6SB^{iii}	2.884	2.852	0.05	0.063	−3.9	1.3	1.22	−0.07
Cl5	**H39**	**2.735**	**2.609**	**0.08**	**0.084**	**−6.6**	**1.1**	**2.07**	**−0.22**
Cl6	H10^{iv}	2.879	2.724	0.06	0.063	−4.6	1.0	1.46	−0.07
	H9^{v}	**2.794**	**2.671**	**0.07**	**0.075**	**−5.3**	**1.3**	**1.67**	**−0.16**
Cl8	H35^{vi}	2.913	2.788	0.05	0.055	−3.4	1.2	1.05	−0.04
	H6SC^{iii}	2.874	2.751	0.06	0.056	−4.0	0.9	1.27	−0.08
Cl9	**C30^{vii}**	**3.351**	**3.369**	**0.04**	**0.049**	−2.9	1.1	**0.90**	**−0.10**
Cl10	H11^{iv}	2.950	2.756	0.06	0.058	−4.1	1.0	1.29	0.00

[a] r_{exp}(A–Z) and r_{theor}(A-Z) are experimental and theoretical interatomic distances (Å); $\rho(\mathbf{r})$ – the ED at the BCP (e Å^{-3}); $\nabla^2\rho(\mathbf{r})$ – the corresponding Laplacian (in e Å^{-5}); $V^e(\mathbf{r})$ – the potential energy density (a.u.); $h_e(\mathbf{r})$ – the local energy density (a.u.); E_{int} – energy for a intermolecular bond estimated using the EML correlation (kcal/mol); Δ – the difference between experimental interatomic distance and van der Waals radii. The Cl atoms involved, according to ^{35}Cl NQR, in secondary interactions are given in bold;
[b] Symmetry codes: (i) −*x*, 2 − *y*, −*z*; (ii) 1 + *x*, −1 + *y*, *z*; (iii) −1 + *x*, 1 + *y*, *z*; (iv) *x*, −1 + *y*, *z*; (v) −2 − *x*, 3 − *y*, 1 − *z*; (vi) −1 − *x*, 2 − *y*, −*z*; (vii) −1 + *x*, *y*, *z*.

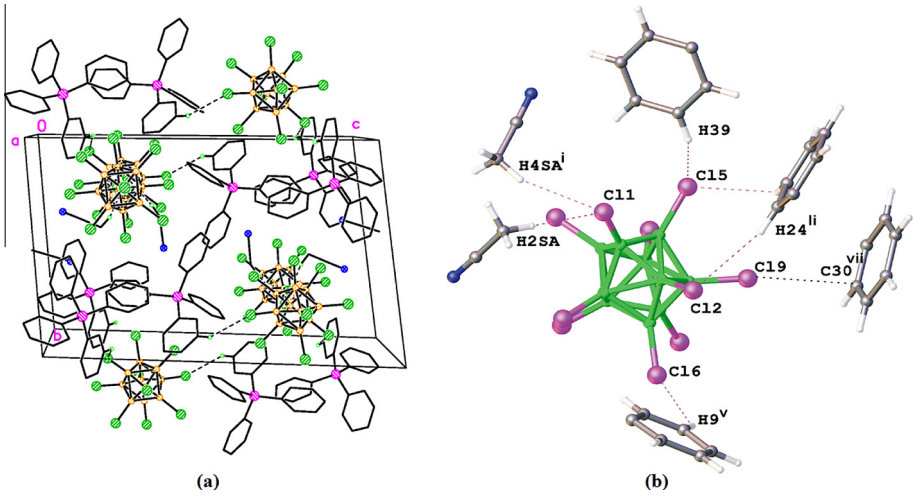

Fig. 6. (a) Fragment of crystal packing of **2** (view along crystallographic axis *a*). Hydrogen atoms not involved in C–H. . .Cl bonding are omitted. (b) Secondary interactions in **2**·3CH_3CN reflected in the ^{35}Cl NQR spectrum. Symmetry codes of the hydrogen and carbon atoms are given in Footnotes to Table 4.

a cubic structure [35]. The results showed that the interaction including ion–ion repulsion and acting through the electron inner shell polarization of the Cl atoms (Sternheimer antishielding) is a dominant factor determining the crystal field effect in these salts. With increasing size of the cation the interionic Cl–Cl distances increase, the repulsion between them weakens, and the Sternheimer antishielding decreases.

As it was found in the present NQR study of the decachloro-*closo*-decaborate ionic compounds, the large size of the anions (and cations) resulted in very similar frequency ranges for the salts of all the cations. That is, the halogen frequencies in the NQR spectra of the discussed clusters are mainly determined by the intraanionic electronic distribution and weakly depend on the cation nature.

Because both technical limitations of the equipment and closely spaced components of the multiplet (Fig. 7) made the measurements of η impossible, we have attempted to estimate them from DFT. The calculated quadrupolar coupling constants (QCC = eQq_{zz}/h) and EFG asymmetry parameters (η) for all the chlorine atoms in **2** and **3** are listed in Table 5.

The resonance frequencies, together with the intensities of the corresponding lines, which are calculated from the values in Table 5, are shown in Figs. 4 and 7 as negative rods on the scale

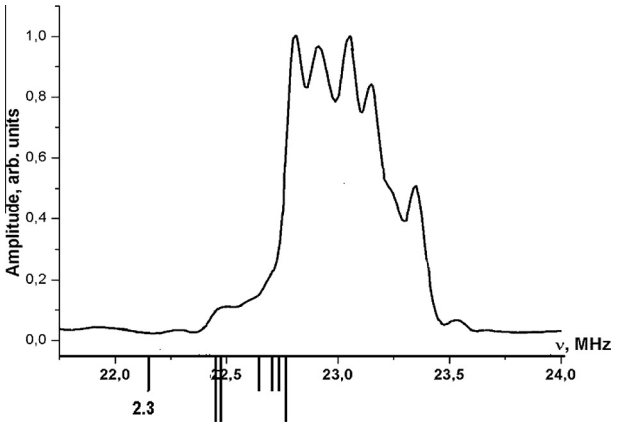

Fig. 7. The ^{35}Cl NQR spectrum of **2**·3CH_3CN at 19 K. The resonance frequencies, estimated from PW-DFT data, are shown as negative rods on the recording of the experimental spectrum. Below one rod, the EFG asymmetry parameter (η, %) is also given.

of the experimental spectra. Although the coincidence with the experiment is poor, one can conclude that the participation of the chlorine atoms in secondary interactions may considerably

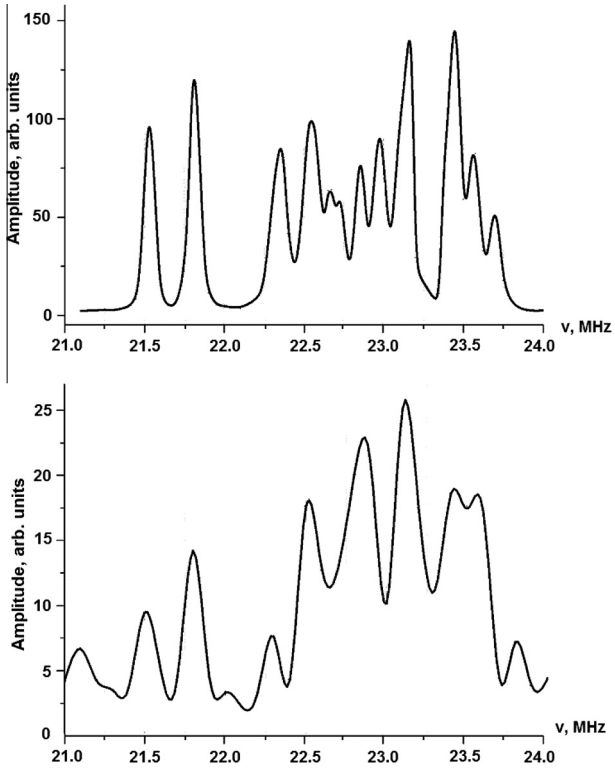

Fig. 8. ^{35}Cl NQR spectrum of **1** at 19 K (a) and 77 K (b).

affect the spectral pattern of the anion making the relative positions of the resonances assigned to apical and equatorial chlorines unpredictable.

Nevertheless, the calculations confirm that the observed NQR spectra allow to select among the whole set of interatomic contacts those, which are caused by secondary interactions (or weak coordination bonding). The formation of these bonds is accompanied by subtle changes in the electron density distribution on the appropriate chlorine atoms resulting in the splitting of these resonances.

Table 6
The electronic characteristics of the Cl atoms in the $[B_{10}Cl_{10}]^{2-}$ anions of compounds **2** and **3** (see text).

	ν^{av}_{exp}, MHz	η^{av}_{calc}, %	eQq/h, MHz	$\pi(Np_x-Np_y)$	$-\rho$, e
2	ν_e22.90	12.95	45.9	0.036	0.53
3	ν_a21.50	8.7	43.0	0.023	0.57
	ν_e22.15	16.4	44.5	0.044	0.53

Table 7
Crystallographic data and refinement parameters for **2**·3MeCN and **3**.

Compound	**2**·3MeCN	**3**
Empirical formula	$C_{54}H_{49}B_{10}Cl_{10}N_3P_2$	$Ag_2B_{10}Cl_{10}H_{12}N_4$
Fw	1264.50	746.48
Color, habit	Colorless, prism	Colorless, needle
Crystal size (mm^3)	0.23 × 0.18 × 0.10	0.42 × 0.08 × 0.07
$F(000)$	1288	1416
T (K)	120	120
Space group	triclinic, $P\bar{1}$	orthorhombic, *Pbcn*
Z	2	4
a (Å)	10.7655(4)	14.4280(19)
b (Å)	13.5998(6)	11.8855(16)
c (Å)	21.8168(9)	13.3806(18)
α (°)	82.218(1)	90
β (°)	79.404(1)	90
γ (°)	76.273(1)	90
V (Å^3)	3035.9(2)	2294.6(5)
d_c (g/cm^3)	1.383	2.161
μ(Mo Kα) (cm^{-1})	0.552	2.868
θ_{max} (°)	30.60	36.32
I_{hkl}coll/unique	56351/18624	38469/5376
R_{int}	0.022	0.064
Obs. refl./N/restraints	16300/715/0	4061/120/0
R,[a] % [$I > 2\sigma(I)$]	0.030	0.043
R_w,[b] %	0.085	0.097
Goodness-of-fit (GOF) on F^2[c]	0.99	0.99
Refcode[d]	1428020	1428019

[a] $R = \Sigma||F_o| - |F_c||/\Sigma|F_o|$.
[b] $R_w = [\Sigma(w(F_o^2 - F_c^2)^2)/\Sigma(w(F_o{}^2))]^{1/2}$.
[c] GOF = $[\Sigma w(F_o^2 - F_c^2)^2/(N_{obs} - N_{param})]^{1/2}$.
[d] Code of compound at the CSD.

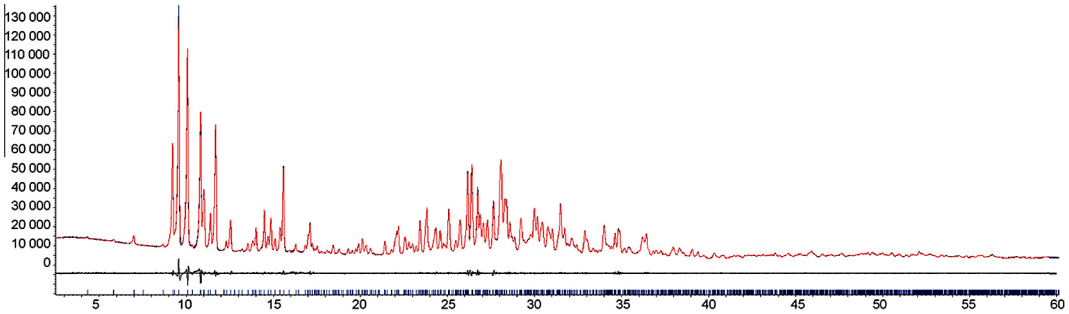

Fig. 9. The experimental (blue) and calculated (red) powder patterns for **1** at room temperature, their difference (black) and theoretical peak sticks for a given unit cell. (For interpretation of the references to color in this figure legend, the reader is referred to the web version of this article.)

Table 5
Theoretical NQR parameters for the chlorine atoms in **2** and **3**.

		Cl1	Cl2	Cl3	Cl4	Cl5	Cl6	Cl7	Cl8	Cl9	Cl10
2	QCC, MHz	−44.3	−45.5	−45.6	−45.4	−45.0	−45.1	−45.6	−45.1	−45.6	−44.9
	η, %	2.3	15.9	10.6	11.1	12.8	14.0	10.7	14.6	13.8	4.1
3	QCC, MHz	−43.2	−44.7	−45.1	−45.4	−44.5					
	η, %	7.9	9.5	20.0	14.6	14.7					

To get a rough picture of the electronic characteristics of the Cl atoms in the anions—the effective negative charges ($-\rho$, e) and difference in the occupation of the valence p_π-orbitals (Np_x–Np_y)—we listed in Table 6 these characteristics estimated using the average values of the experimentally measured frequencies (ν^{av}_{exp}, MHz) and calculated (see Table 5) EFG asymmetry parameters (η^{av}_{calc}, %). It is evident, that (Np_x–Np_y) gives the value of π-character if the charge transfer occurs from one of the chlorine p_π-orbitals, whereas the occupation number of the other (Np_x or Np_y) does not change.

4. Conclusions

The results of ^{35}Cl NQR studies of decachloro-*closo*-decaborates $R_2[B_{10}Cl_{10}]$, where R are Et_3NH^+, Ph_4P^+, and $[Ag(NH_3)^2]^+$ supported by PW-DFT calculations and the QTAIM analysis showed that the NQR spectral patterns allow to select from the whole set of interatomic contacts, determined by X-ray diffraction studies, those which are caused by secondary interactions (weak coordination bonding). The formation of these bonds is accompanied by subtle changes in the electron density distribution on the appropriate chlorine atoms resulting in the splitting of the appropriate resonances. A direct correlation was found to exist between the interaction energy and ^{35}Cl NQR spectroscopic characteristics of associates of $[B_{10}Cl_{10}]^{2-}$ cluster with midsize cations and molecules. The results showed that the halogen-substituted boron clusters are capable of producing H...Hal and p...π bonds, which can be identified by NQR spectra even in the absence of structural data.

5. Experimental

5.1. Synthetic procedures

Organic solvents and liquid organic reagents were purified and dried according to the standard procedures. All the reactions were carried out in air. $[HNEt_3]_2[B_{10}H_{10}]$ was synthesized from decaborane-14 according to the known procedure [36]. Chlorination of $K_2[B_{10}H_{10}]$ by chlorine in water to form $K_2[B_{10}Cl_{10}]$ was reported in Ref. [11].

5.1.1. $[HNEt_3]_2[B_{10}Cl_{10}]$ (**1**)

A solution of $K_2[B_{10}Cl_{10}]$ (3 mmol) in water (5 ml) was added to a solution of $[HNEt_3]Cl$ (6 mmol) in water (5 ml). Compound **1** precipitates from the reaction solution after 24 h, it was filtered off, washed out by water (3 × 5 ml), and dried in air. The yield was 91%. *Anal.* Calc. for $C_{12}H_{30}N_2B_{10}Cl_{10}$ (**1**): C, 21.67; H, 4.55; N, 4.21; B, 16.26; Cl, 53.31. Found: C, 21.52; H, 4.44; N, 4.11; B, 16.15; Cl, 53.27%. **IR** (ν, cm^{-1}): ν(NH) 3147, 3168; ν(BCl) 1156, 1003; δ(HCH) 1460–720 cm^{-1}. ^{11}B NMR ([D_7]DMF): δ = 4.44 (2B, s, B_{ap}); −2.85 (8B, s, B_{eq}).

5.1.2. $(Ph_4P)_2[B_{10}Cl_{10}]$ (**2**)

A solution of $[HNEt_3]_2[B_{10}Cl_{10}]$ (**1**) (3 mmol) in water (5 ml) was added to a solution of $[Ph_4P]Cl$ (6 mmol) in water (5 ml). Qualitative precipitation of **2** was observed immediately. The obtained precipitate was filtered off, washed out by water (3 × 5 ml), and dried in air. *Anal.* Calc. for $C_{48}H_{40}P_2B_{10}Cl_{10}$ (**2**): C, 50.51; H, 3.53; B, 9.47. Found: C, 50.43; H, 3.44; B, 9.37%. IR (ν, cm^{-1}): ν(BCl) 1158, 999; δ(HCH) 1460–720 cm^{-1}. ^{11}B NMR ([D_7]DMF): δ = 4.21 (2B, s, B_{ap}); −2.68 (8B, s, B_{eq}).

5.1.3. $[Ag(NH_3)_2]_2[B_{10}Cl_{10}]$ (**3**)

A solution of $AgNO_3$ (4 mmol) in water (5 ml) was added to a solution of $[HNEt_3]_2[B_{10}Cl_{10}]$ (**1**) (2 mmol). A solution of NH_3 H_2O (8 mmol) was added to the obtained reaction solution. Formation of colorless needle crystals **3** was observed for 24 h. The obtained crystals were filtered off, washed out by water (3 × 5 ml), and dried in air. The yield was about 85%. *Anal.* Calc. for $Ag_2N_4H_{12}B_{10}Cl_{10}$ (**1**): Ag, 28.90; N, 7.51; H, 1.62; B, 14.48. Found: Ag, 28.81; N, 7.42; H, 1.51; B, 14.32%. IR (ν, cm^{-1}): ν(NH) 3380, 3289; δ(HNH) 1674, 1601; ν(BCl) 1163, 1003; δ(HCH) 1460–720 cm^{-1}. ^{11}B NMR ([D_7]DMF): δ = 4.15 (2B, s, B_{ap}); −2.54 (8B, s, B_{eq}).

5.2. Materials and methods

Elemental analysis was carried out on an EA 1108 automatic CHN analyzer (Carlo Erba Instruments). All the samples were dried under vacuum at room temperature to constant weight to obtain solvent-free compounds. Determination of boron was performed by electrothermal atomic absorption on a Perkin–Elmer 2100 spectrophotometer with an HGA-700 furnace [37]. Silver was determined on a Perkin–Elmer 303 atomic absorption spectrophotometer in an acetylene-air flame on 248.3 nm analytical wave length; lamp current 25 mA, hollow cathode lamp (Carl Zeiss). The powder patterns of **1**–**3** were measured on a Bruker D8 Advance Vario diffractometer at RT with LynxEye detector and Ge (111) monochromator, λ(Cu Kα_1) = 1.54060 Å, $\theta/2\theta$ scan from 5.5° to 60° (**2** and **3**) or from 1.8° to 90° (**1**), step size 0.01°. The measurement was performed in transmission mode, with the sample deposited between two Kapton films. The patterns were index directly to confirm absence of phase transitions or impurities. Results of PXRD for **2** and **3** are given in Supplementary.

IR spectra of compounds **1**–**3** were recorded on an InfraLUM FT-02 FT-IR spectrometer (Lumex, St.-Petersburg, Russia) in the range of 600–4000 cm^{-1} (Nujol mull, NaCl pellets).

^{11}B NMR spectra of compounds **1**–**3** in [D_7]DMF were recorded on a Bruker AC 200 spectrometer at a frequency of *64.297* MHz using $BF_3{\cdot}Et_2O$ as an external standard.

Single crystal of complex **3** was isolated directly from the reaction solution, that of salt **2**·3MeCN was obtained by the recrystallization of precipitate **2** from acetonitrile solution. The intensities of reflections were measured with a Bruker Apex II CCD diffractometer using Mo Kα (λ = 0.71073 Å) radiation. The structures were solved by the direct method and refined by full-matrix least squares against F^2. Hydrogen atoms were included in the refinement by the riding model with U_{iso}(H) = nU_{eq}(C), where n = 1.5 for methyl groups and 1.2 for the rest atoms. All calculations were performed using SHELXL 2013 [38] and OLEX 2.0 [39] program packages. Crystallographic data and refinement parameters for **3** and **2**·3MeCN are presented in Table 7.

^{35}Cl NQR measurements were performed at 19 and 77 K utilizing a home-built phase coherent pulsed NMR/NQR spectrometer. The ^{35}Cl NQR spectra were measured using a frequency step point-by-point spin-echo technique. At each frequency point, the area under the spin-echo magnitude was integrated in the time domain and averaged by a number of accumulations, which depends on the sample and temperature. Unfortunately, the instrument has no adjustment for registering the NQR spin-echo envelope in external magnetic fields (the sample is inserted into the transport vessel with liquid helium). The measurement of the EFG asymmetry parameter is based on Fourier analysis of slow beats of the spin-echo envelope in an external magnetic field. In more detail, the approach is described in Ref. [40].

It is important to note that the ^{35}Cl NQR spectra of **1**–**3** could be observed only after cooling the samples to 19 K. We could also observe the spectrum of **3** at 77 K, but a thorough search of the ^{35}Cl resonances at room temperature gave no results for all the samples.

The quantum chemical calculations of the crystalline state of **2** and **3** were carried out using the Vienna Ab-initio Simulation Package (VASP) 4.6.28 code [41]. Conjugated gradient technique was used for optimizations of the atomic positions (started from

experimental data) and minimization of total energy. Projected augmented wave (PAW) method was applied to account for core electrons while valence electrons were approximated by plane-wave (PW) expansion with 800 eV cutoffs. Exchange and correlation terms of total energy were described in terms of density functional theory (DFT). PBE exchange-correlation functional was used for this purpose [42]. At a final step of our calculations atomic displacements converged were better than 0.01 eV $Å^{-1}$, as well as energy variations were less than 10^{-3} eV. In order to carry out the topological analysis of electron density distribution function in terms of AIM theory the dense (stepsize between grid points is equal to 0.025 Å) FFT (fast Fourier transformation) grid was used. The latter was obtained by separate single point calculation of optimized geometry with small core PAWs for each atom type. The topological analysis of electron density distribution function was carried out using AIM program—part of ABINIT software package [43].

Acknowledgments

The synthesis and ^{35}Cl NQR spectroscopy studies of compounds **1**–**3** were supported by the Federal Agency of Scientific Organizations (0088-2014-0001). A.V.V. and A.A.K. acknowledge the financial support of the Russian Science Foundation (Grant 14-13-00884) for PW-DFT calculations of **2** and **3**.

Appendix A. Supplementary material

Supplementary data associated with this article can be found, in the online version, at http://dx.doi.org/10.1016/j.ica.2016.03.025.

References

[1] (a) E.L. Muetterties, J.H. Balthis, Y.T. Chia, W.H. Knoth, H.C. Miller, Inorg. Chem. 3 (1964) 444;
(b) E.L. Muetterties, W.H. Knoth, Polyhedral Boranes, Dekker, New York, 1968;
(c) N.N. Greenwood, A. Earnshaw, Chemistry of the Elements, 2., Butterworth-Heinemann, 1997;
(d) I.B. Sivaev, A.V. Prikaznov, D. Naoufal, Collect. Czech. Chem. Commun. 75 (2010) 1149;
(e) E.A. Malinina, V.V. Avdeeva, L.V. Goeva, N.T. Kuznetsov, Russ. J. Inorg. Chem. 55 (2010) 2148;
(f) M. Driess, H. Noth, Molecular Clusters of the Main Goup Elements, Wiley VCH Verlag GmbH & Co, 2005;
(g) R.N. Grimes, J. Organomet. Chem. 747 (2013) 4.
[2] (a) E.A. Malinina, V.V. Avdeeva, L.V. Goeva, I.N. Polyakova, N.T. Kuznetsov, Russ. J. Inorg. Chem. 56 (2011) 687;
(b) E.A. Malinina, L.V. Goeva, N.T. Kuznetsov, Russ. J. Inorg. Chem. 54 (2009) 417;
(c) O.A. Filippov, N.V. Belkova, L.M. Epstein, E.S. Shubina, J. Organomet. Chem. 747 (2013) 30;
(d) A.V. Virovets, N.N. Vakulenko, V.V. Volkov, N.V. Podberezskaya, Zh. Struct. Khim. 35 (3) (1994) 72.
[3] (a) A.N. Deyand, J. Miller, J. Electrochem. Soc. 126 (1979) 1445;
(b) J. Johnson, M. Whittingham, J. Electrochem. Soc. 127 (1980) 165;
(c) J. Johnson, A. Thompson, J. Electrochem. Soc. 128 (1981) 932;
(d) J. Brody, J. Electrochem. Soc. 729 (1982) 2213.
[4] (a) M. Nieuwenhuyzen, K.R. Seddon, F. Teixidor, A.V. Puga, C. Vinas, Inorg. Chem. 48 (2009) 889;
(b) B. Ringstrand, A. Balinski, A. Franken, P. Kaszynski, Acc. Chem. Res. 46 (2013) 214.
[5] (a) C.-W. Tsang, Q. Yang, E.T.-P. Sze, T.C.W. Mak, D.T.W. Chan, Z. Xie, Inorg. Chem. 39 (2000) 5851;
(b) R. Ramírez-Contreras, N. Bhuvanesh, J. Zhou, O. Ozerov, Angew. Chem., Int. Ed. 52 (2013) 10313.
[6] (a) E.S. Stoyanov, S.P. Hoffmann, M. Juhasz, C.A. Reed, J. Am. Chem. Soc. 128 (2006) 3160;
(b) E.S. Stoyanov, G. Gunbas, N. Hafezi, M. Mascal, I. Stoyanova, F.S. Tham, C.A. Reed, J. Am. Chem. Soc. 134 (2012) 707;
(c) A. Avelar, F.S. Tham, C.A. Reed, Angew. Chem., Int. Ed. 48 (2009) 3491.
[7] M.W. Rupich, J.S. Foos, S.B. Brummer, J. Electrochem. Soc. 132 (1985) 119.
[8] N.W. Alcock, Adv. Inorg. Chem. Radiochem. 15 (1972) 1.
[9] (a) Y.A. Buslaev, E.A. Kravchenko, L. Kolditz, Coord. Chem. Rev. 82 (1987) 1;
(b) Proceedings of Joint International Conferences on Hyperfine Interactions & Nuclear Quadrupole Interactions (HFI/NQI): Hyperfine Interactions, 2005, vols. 158–159; 2007(180), 2010, 197. HFI/NQI, 2012, Eds. S. Zhu, G. Zhang, F. Li and D. Yuan.;
(c) J. Kubišta, M. Civiš, P. Španěl, S. Civiš, Analyst 137 (2012) 1338;
(d) S. Pérez, A. Wolfenson, Solid State Nucl. Magn. Reson. 41 (2012) 68;
(e) K.E. Johnston, C.A. O'Keefe, R.M. Gauvin, J. Trébosc, L. Delevoye, J.-P. Amoureux, N. Popoff, M. Taoufik, K. Oudatchin, R.W. Schurko, Chem. Eur. J. 19 (2013) 12396;
(f) P. Ingman, G.W. Driver, Phys. Chem. Chem. Phys. 14 (37) (2012) 13053;
(g) Y. Tobu, R. Ikeda, T.-A. Nihei, K. Gotoh, H. Ishida, A. Tetsuo, Phys. Chem. Chem. Phys. 14 (2012) 12347.
[10] A. Weiss, Fortschr. Chem. Forsch. 30 (3) (1972) 3.
[11] W.H. Knoth, H.C. Miller, J.C. Sauer, J.H. Balthis, Y.T. Chia, E.L. Muetterties, Inorg. Chem. 3 (1964) 159.
[12] (a) W. Einholz, K. Vaas, C. Wieloch, B. Speiser, T. Wizemann, M. Ströbele, H.-J. Meyer, Z. Anorg, Allg. Chem. 628 (2002) 258;
(b) W. Bowden, J. Electrochem. Soc. 129 (1982) 1249.
[13] (a) L. Zhang, P. Hu, J. Xiang, G. Zhang, J. Wuhan. Univ. (Nat. Sci. Ed.) 2 (1985) 59;
(b) Y.L. Gaft, N.T. Kuznetsov, Russ. J. Inorg. Chem. 26 (1981) 699;
(c) Y.L. Gaft, I.A. Zakharova, N.T. Kuznetsov, Russ. J. Inorg. Chem. 25 (1980) 726;
(d) A.M. Orlova, L.V. Goeva, K.A. Solntsev, N.T. Kuznetsov, Zh. Neorg. Khim. 41 (1996) 796;
(e) N.T. Kuznetsov, L.A. Zemskova, Zh. Neorg. Khim. 27 (1982) 1320.
[14] V.V. Avdeeva, A.V. Vologzhanina, L.V. Goeva, E.A. Malinina, N.T. Kuznetsov, Inorg. Chim. Acta 428 (2015) 154.
[15] L. Pang, E.A.C. Lucken, G. Bernardinelli, J. Am. Chem. Soc. 112 (24) (1990) 8754.
[16] S. Limandri, C. Visñovezky, S.C. Perez, C.A. Schurrer, A.E. Wolfenson, M. Ferro, S. L. Cuffini, J. Goncalves de Souza, F.A. Aguiarand, C. Masetto de Gaitani, Anal. Chem. 83 (5) (2011) 1773.
[17] G. Wulfsberg, K.D. Parks, R. Rutherford, D. Jackson, F.E. Jones, D. Derrick, W. Ilsley, S. Strauss, S. Miller, O.P. Anderson, T.A. Babushkina, S.I. Gushchin, E.A. Kravchenko, V.G. Morgunov, Inorg. Chem. 41 (2002) 2032.
[18] F.H. Herbstein, Cryst. Growth Des. 5 (6) (2005) 2362.
[19] R.F.W. Bader, Atoms in Molecules – A quantum theory, Oxford University Press, New York, 1990.
[20] (a) I. Alkorta, I. Rozas, J.N. Elguero, J. Phys. Chem. A 102 (1998) 9278;
(b) Y.-X. Lu, J.-W. Zou, Y.-H. Wang, Y.-J. Jiang, Q.-S. Yu, J. Phys. Chem. A 111 (42) (2007) 10781;
(c) S. Grabowski, J. Phys. Chem. A 2012 (1838) 116;
(d) O.A. Syzgantseva, V. Tognetti, L. Joubert, J. Phys. Chem. A 117 (2013) 8969.
[21] J. Seliger, V. Žagar, J.N. Latosińska, Phys. Chem. Chem. Phys. 12 (2010) 13007.
[22] I. Tiritiris, T. Schleid, Z. Anorg, Allg. Chem. 629 (2003) 581.
[23] E.D. Jemmis, G. Subramanian, I.H. Srivastava, J. Phys. Chem. 98 (1994) 6445.
[24] S. Mebs, R. Kalinowski, S. Grabowski, D. Förster, R. Kickbusch, E. Justus, W. Morfenroth, C. Paulmann, P. Luger, D. Gabel, D. Lentz, Inorg. Chem. 50 (1) (2011) 90.
[25] A.V. Vologzhanina, A.A. Korlyukov, V.V. Avdeeva, I.N. Polyakova, E.A. Malinina, N.T. Kuznetsov, J. Phys. Chem. A 117 (2013) 13138.
[26] R.F.W. Bader, D.A. Legare, Can. J. Chem. 70 (1992) 657.
[27] E. Espinosa, E. Molins, C. Lecomte, Chem. Phys. Lett. 285 (1998) 170.
[28] (a) A.O. Borissova, A.A. Korlyukov, M.Y. Antipin, K.A. Lyssenko, Phys. Chem. A 112 (2008) 11519;
(b) L.N. Puntus, K.A. Lyssenko, M.Y. Antipin, J.-C.G. Bünzli, Inorg. Chem. 47 (2008) 11095;
(c) A. Tikhonova, K.I. Tugashov, F.M. Dolgushin, A.A. Korlyukov, P.V. Petrovskii, Z.S. Klemenkova, V.B. Shur, J. Organomet. Chem. 694 (2009) 2604;
(d) I.V. Ananyev, S.E. Nefedov, K.A. Lyssenko, Eur. J. Inorg. Chem. (2013) 2736;
(f) A.V. Vologzhanina, K.A. Lyssenko, Rus. Chem. Bull. 62 (2013) 1786;
(g) K.A. Lyssenko, A.V. Vologzhanina, Y.V. Torubaev, Y.V. Nelyubina, Mendeleev Commun. 24 (2014) 216.
[29] H. El Aribi, C.F. Rodriquez, T. Shoeib, T. Shoeib, Y. Ling, A.C. Hopkinson, K.W. Michael Siu, J. Phys. Chem. A 106 (2002) 8798.
[30] H. Dengand, P. Kebarle, J. Phys. Chem. A 102 (3) (1998) 571.
[31] Blatov et al., Cryst. Growth Des. 14 (2014) 3576.
[32] (a) A. Bondi, J. Phys. Chem. 68 (3) (1964) 441;
(b) A. Bondi, J. Phys. Chem. 70 (9) (1966) 3006.
[33] M. Cohen, Phys. Rev. 96 (1954) 1278.
[34] E.A. Kravchenko, M.Y. Burtzev, A.V. Yatsenko, L.A. Aslanov, Main Group Metal Chem. 20 (5) (1997) 339.
[35] (a) T.B. Brill, R.G. Gearhart, W.A. Welsh, J. Magn. Res. 13 (1974) 27;
(b) T.B. Brill, J. Chem. Phys. 61 (1974) 424;
(c) R. Ikeda, A. Sasane, D. Nakamura, M. Kubo, J. Phys. Chem. 70 (9) (1966) 2926.
[36] H.C. Miller, N.E. Miller, E.L. Muetterties, J. Am. Chem. Soc. 85 (1963) 3885.
[37] L.I. Ochertyanova, V.N. Mustyatsa, K.Yu. Zhizhin, O.N. Belousova, N.T. Kuznetsov, Inorg. Mater. 40 (2004) 144.
[38] G.M. Sheldrick, Acta Crystallogr. Sect. C 71 (2015) 3.
[39] O.V. Dolomanov, L.J. Bourhis, R.J. Gildea, J.A.K. Howard, H. Puschmann, J. Appl. Crystallogr. 42 (2009) 339.
[40] E.A. Kravchenko, Yu.A. Buslaev, Russ. Chem. Rev. 68 (9) (1999) 709.
[41] (a) G. Kresse, J. Hafner, Phys. Rev. B 47 (1993) 558;
(b) G. Kresse, J. Furthmüller, Phys. Rev. B 54 (1996) 11169;
(c) G. Kresse, J. Furthmüller, Comput. Mater. Sci. 6 (1996) 15.
[42] J.P. Perdew, K. Burke, M. Ernzerhof, Phys. Rev. Lett. 77 (1996) 3865.
[43] X. Gonze, J.-M. Beuken, R. Caracas, F. Detraux, M. Fuchs, G.-M. Rignanese, L. Sindic, M. Verstraete, G. Zerah, F. Jollet, M. Torrent, A. Roy, M. Mikami, Ph. Ghosez, J.-Y. Raty, D.C. Allan, Comput. Mater. Sci. 25 (2002) 478.